JOM
DOI: 10.1007/s11837-017-2411-x

Interfacial Fracture of Nanowire Electrodes of Lithium-Ion Batteries

G.R. HARDIN,[1] Y. ZHANG,[1] C.D. FINCHER,[1] and M. PHARR[1,2]

1.—Department of Mechanical Engineering, Texas A&M University, 3123 TAMU, College Station, TX 77843, USA. 2.—e-mail: mpharr85@tamu.edu

Nanowires (NW) have emerged as a promising design for high power-density lithium-ion battery (LIB) electrodes. However, volume changes during cycling can lead to fracture of the NWs. In this paper, we investigate a particularly detrimental form of fracture: interfacial detachment of the NW from the current collector (CC). We perform finite element simulations to calculate the energy release rates of NWs during lithiation as a function of geometric parameters and mechanical properties. The simulations show that the energy release rate of a surface crack decreases as it propagates along the NW/CC interface toward the center of the NW. Moreover, this paper demonstrates that plastic deformation in the NWs drastically reduces stresses and thus crack-driving forces, thereby mitigating interfacial fracture. Overall, the results in this paper provide design guidelines for averting NW/CC interfacial fractures during operation of LIBs.

INTRODUCTION

New technologies powered by lithium-ion batteries (LIB) demand greater capacities, longer cycle lives, and lower costs.[1–4] In response, researchers have identified a number of candidate high-capacity electrode materials. Unfortunately, as a general principle, the more lithium an electrode can absorb, the more it will swell.[5] For example, silicon has an enormous gravimetric capacity of 3579 mAh/g, but it swells approximately 300% upon lithiation.[5,6] Under constraint, these large strains generate stresses, which can lead to fracture of the electrode.[6–8] Fractured electrodes exhibit large electrical resistivity, may lose electrical contact with the current collector (CC), and provide a more surface area for solid electrolyte interphase (SEI) growth, all of which lead to capacity fade.[9–12]

To address these issues, electrodes are often nano-structured in the form of thin films, nanopillars, nanoparticles, or nanowires (NWs).[13–15] NWs are particularly popular due to the open space between them into which individual NWs can freely swell, thereby reducing stresses in the electrodes.[16,17] These configurations also introduce shorter diffusion distances for the Li-ions, thus enabling high charge/discharge rates.[14,18,19] However, despite their advantages, NWs can still suffer mechanical degradation. For instance, Nguyen et al. found Si NWs floating in the electrolyte after cycles of lithiation/de-lithiation due to detachment of the NWs from the CC.[17] In addition to Si, NW electrodes of Ge, Co_3O_4, TiO_2, and SnO_2 have been implemented in LIBs.[20–24]

Despite the prevalence of NWs in LIBs, only a few studies have analyzed the mechanics of their fracture. Ryu et al. studied lithiation of Si NWs and found a critical radius of 300 nm, below which internal fracture was averted in both simulation and experiment.[25] Liu et al.[26] also studied lithiated Si NWs and found anisotropic swelling under certain conditions, which resulted in large tensile hoop stresses which propagated internal cracks. While internal fractures of NWs have been studied, no mechanical studies have addressed a separate key concern: lithiation-induced detachment of the NW from the CC. During lithiation, the NW expands but the CC does not. As a result, stresses are generated near the root of the NW, which may lead to detachment from the CC, thus diminishing the capacity of the battery.[17]

G.R. Hardin and Y. Zhang have contributed equally to this manuscript.

Published online: 12 June 2017

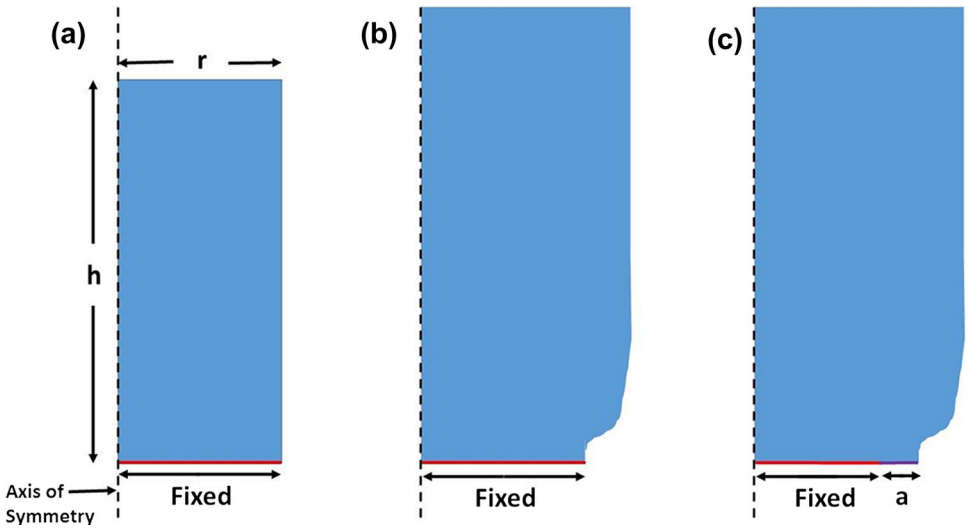

Fig. 1. Schematics of a nanowire during the ABAQUS simulations. (a) The nanowire prior to lithiation and corresponding dimensions. (b) The nanowire as it expands during lithiation. The nanowire is fixed along the interface with the current collector, and the strain energy, U_1, is computed. (c) A free surface of length a is introduced to represent a crack. The strain energy, U_2, is calculated. The difference between the strain energies in (b) and (c) determines the crack driving force through Eq. 1.

This paper analyzes detachment of NW electrodes from CCs during electrochemical cycling. We implemented finite element simulations to calculate the energy release rate associated with the propagation of a surface flaw during lithiation. The simulations also reveal the dependence of the energy release rate on the crack length, aspect ratio, NW radius, and yield strength. Overall, the results in this paper provide design guidelines for averting NW/CC interfacial fractures during operation of LIBs.

NUMERICAL PROCEDURE

To simulate interfacial fractures along the NW/CC interface, we performed finite element simulations in ABAQUS. The NW electrode is represented by an axisymmetric model of length h, radius r, and surface-crack length a, as shown in Fig. 1. Here, we implement an axisymmetric model for simplicity due to the absence of experimental data regarding the precise shape of the flaws at the NW/CC interface. Additionally, the crack driving force depends primarily on the length of the crack and less so on the precise shape (e.g., the width of the crack). During the initial step, the base of the NW was fixed to represent the constraint that the CC places on it. With this constraint in place, the NW swells due to the insertion of the lithium. We simulate this step by implementing thermal swelling to the same level of volume expansion associated with lithiation of the material (Fig. 1b). As an example, Si swells by ~280% upon lithiation to the fully lithiated state of $Li_{3.75}Si$;[27,,28] a corresponding level of thermal strain was implemented to simulate these conditions, with large deformation taken into account (Nlgeom enabled in ABAQUS). In this step, it is assumed that enough time is allowed for diffusive equilibrium (e.g., as during slow charging) such that the concentration of lithium is uniform in the NW. We make this assumption due to the mechanics of the constraint of the CC near the NW/CC interface; large stresses develop near this interface regardless of the precise lithiation kinetics. Likewise, we do not consider the effects of a two-phase reaction-controlled process, as have been observed in some studies.[29–32] In the final step, a crack of length a is introduced by opening a free surface of length a, starting at the surface of the NW and propagating along the NW/CC interface, as shown in Fig. 1c. The length of the crack is incrementally increased toward the center of the NW. During each step, ABAQUS computes the stresses and strains in the NW. The constitutive model employed in ABAQUS is essentially elastic-perfect-plastic but with a small amount of artificial strain hardening added to mitigate numerical issues in the simulation, i.e., to ensure convergence.

To calculate the crack driving force, we follow a method developed by Choi et al.[33] in the context of thin film silicon anodes. They successfully calculated the energy release rate in ABAQUS by computing the incremental change in the internal energy as the crack advances by a unit area. The energy release rate, G, is calculated as follows:

$$G = -\frac{\partial U}{\partial A} = -\frac{U_i - U_{i-1}}{A_i - A_{i-1}} \quad (1)$$

where U_i represents the internal energies in the system when a crack is of a certain length (at step i) and A_i the areas of the uncracked regions at the same step, i.e., the quantity $(A_i - A_{i-1})$ represents

the area swept out by the crack during step i. In ABAQUS, the internal energy includes both the recoverable strain energy as well as the energy dissipated by plastic deformation.

Following standard practice,[34] the crack driving force can also be written in the form:

$$G = Z\bar{E}\varepsilon^2 a \tag{2}$$

where Z is a pre-factor that is a function of non-dimensional variables, $\bar{E} = E/(1-\nu^2)$ is the plane strain modulus, ν the Poisson's ratio, ϵ the strain (in this case from thermal strain), and a the length of the crack. In this study, we will primarily examine the effects of non-dimensional parameters contained in the pre-factor, $Z = f(\frac{\sigma_Y}{E}, \frac{a}{R}, \frac{h}{R})$, on the energy release rate. The three non-dimensional parameters represent the effect of plasticity, crack size (or NW radius), and aspect ratio, respectively, on the energy release rate.

RESULTS AND DISCUSSION

Figure 2 shows the energy release rate as a function of crack size after full lithiation of a Si NW, which corresponds to 280% volume expansion. The NW had a radius of 200 nm, a height of 600 nm, and the material properties listed in Table I.[35] The horizontal line in Fig. 2 indicates an interfacial fracture energy of Γ_i = 1.5 J/m^2, which is representative of the interfacial energy of a $Li_{3.75}Si$/Cu interface.[36] The simulation models the evolution of the crack driving force as the crack advances incrementally toward the center of the NW. As can be seen in Fig. 2, the energy release rate monotonically decreases to zero as the crack advances toward the center of the NW. This phenomenon occurs because, as the crack length approaches the radius of the NW, most of the stresses in the NW have already been relaxed, and thus the crack driving force has diminished. This result represents a key advantage of a NW electrode. That is, from our modeling, we predict that a NW will never completely delaminate from the CC due to lithiation alone. Specifically in our simulation of a fully lithiated silicon NW, propagation of a crack is no longer energetically favorable once $G < \Gamma_i$, represented by the intersection of the black curve with the horizontal red dashed curve in Fig. 2. At this point, the crack will arrest and the NW will not completely delaminate from the CC.

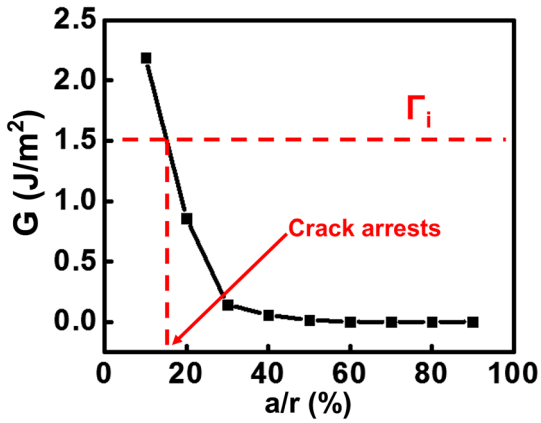

Fig. 2. The energy release rate as a function of crack length (normalized by the radius of the NW) after full lithiation of a Si NW. The horizontal red dashed line indicates a representative value of the interfacial fracture energy of a $Li_{3.75}Si$/Cu interface.

Even if our simulations predict that a NW never entirely delaminates from the CC, crack propagation still has detrimental effects on the system. Crack propagation decreases the contact area between the NW and the CC. As a result, the area of the conducting path for electrons from the CC to the NW decreases, thereby increasing the resistance of the electrode. Similarly, if the crack propagates a large distance, only a small ligament remains that connects the NW to the CC. The remaining NW will be much more susceptible to full debonding due to subsequently applied external loads.

As an additional note regarding Fig. 2, we also simulated Si NWs lithiated to various states of charge. We found that the maximum energy release rate occurs upon full lithiation, so this paper focuses on this critical worst-case scenario. We also simulated de-lithiation of a Si NW and found that the maximum energy release rates were much smaller than during lithiation. As a result, here, we focus on lithiation.

We also performed simulations to evaluate the influence of the mechanical properties of the NW on interfacial fracture. To do so, we varied the yield strength in the simulations relative to the elastic modulus; the results are shown for a NW with a 200-nm radius and a 600-nm height for 10% volume expansion in Fig. 3. For reference, from Table I, $Li_{0.47}Si$ has a value of σ_Y/E = 1.4%. Figure 3 clearly indicates that the crack driving force increases monotonically with the yield strength of the

Table I. Mechanical properties of lithiated silicon

	Li_0Si	$Li_{0.47}Si$	$Li_{1.47}Si$	$Li_{2.34}Si$	$Li_{3.28}Si$	$Li_{3.75}Si$
Young's modulus E (GPa)	113	59	50	43	32	32
Yield strength σ_Y (MPa)	166	800	540	460	340	340
Poisson's ratio (v)			0.25			

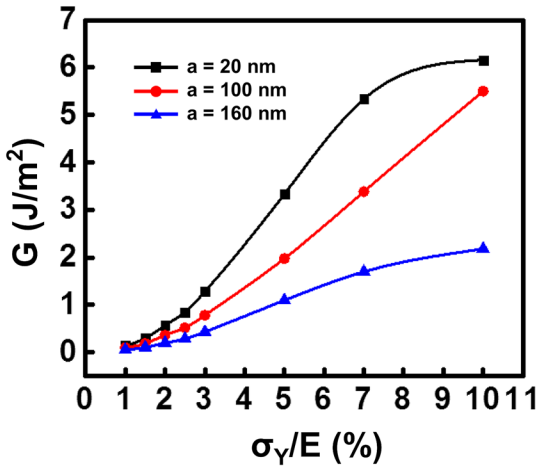

Fig. 3. The energy release rate as a function of the yield strength (normalized by the elastic modulus) for h/r = 3 and volumetric expansion of 10%.

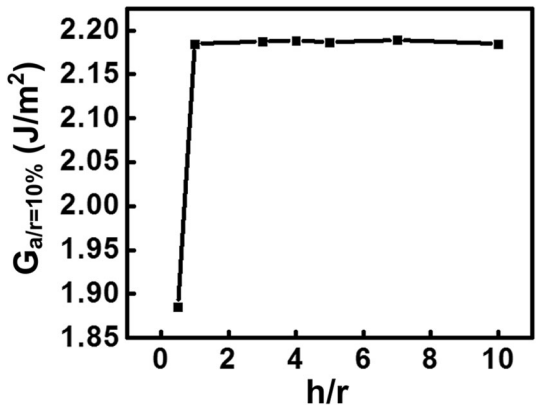

Fig. 4. The maximum energy release rate as a function of the aspect ratio of fully lithiated Si NW.

material. This phenomenon occurs because the NWs are subjected to large swelling strains during lithiation. However, the yield strength of the NW sets a bound on the stress that can build up in the system. Smaller stresses due to smaller yield strengths result in smaller crack driving forces, as there is less stress to relax in the system.

Figure 4 demonstrates the influence of the aspect ratio of the NW, h/r, on the energy release rate for a fully lithiated Si NW. The plot shows the energy release rate for a specific value of $a/r = 10\%$ ($G_{a/r=10\%}$) as a function of crack length. In the simulation, we used the material properties in Table I. The key feature of this plot is that the energy release rate plateaus to a constant value above an aspect ratio of around h/r = 1. In other words, the energy release rate of a NW (for which $h/r \gg 1$) does not depend on the aspect ratio of the NW. Thus, all the simulations performed in this work apply equally well to NWs of any aspect ratio. The phenomenon can be explained by considering

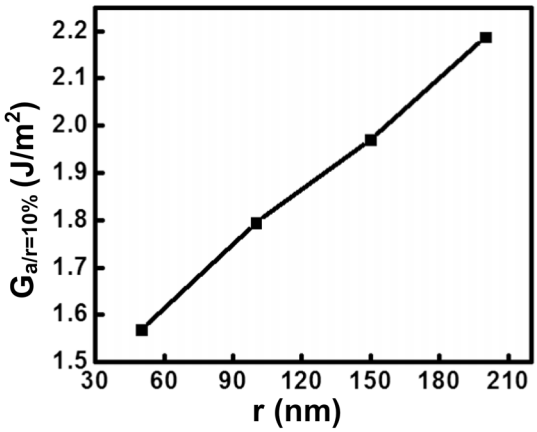

Fig. 5. The maximum energy release rate as a function of the radius of a fully-lithiated Si NW with an aspect ratio of h/r = 3.

the mechanics of the constraint placed on the NW by the CC. Stresses exist near the NW/CC interface in a region whose height scales with the radius of the NW. At distances (in the vertical direction) larger than this, the NW is stress-free. Thus, making the NW taller only adds unstressed regions to the NW and thus does not contribute to the energy release rate. As a final note related to Fig. 4, we should comment that in the previous analyses (e.g., Figs. 2 and 3), we have used a relatively small aspect ratio of $h/r = 3$. However, Fig. 4 demonstrates that even this small aspect ratio is already in the plateau region. Thus, the previous simulations (Figs. 2 and 3) are indeed representative of the physics of a NW.

Although the aspect ratio does not influence the energy release rate, the radius itself does. Figure 5 shows the dependence of the crack driving force (at a particular value of $a/r = 10\%$) on the radius of the NW. We use the material properties listed in Table I and a fixed aspect ratio of $h/r = 3$ in the simulations. The plot shows that the energy release rate scales linearly with the radius of the NW. This result is intuitive in that the volume over which energy is dissipated when a crack advances across the entire CC/NW interface should scale as r^3, while the area of the crack scales as r^2, thus leading to a linear scaling of the crack driving force with the radius of the NW (for a fixed value of h/r). As mentioned previously, crack propagation has detrimental effects on the electrode and thus should be avoided.

CONCLUDING REMARKS

Using finite element simulations in ABAQUS, we have investigated fractures at the interface between a NW electrode and a CC in LIBs as a function of geometric and material parameters. We have found that the energy release rate decays to zero as the crack length approaches the radius of the NW. As a result, the crack either (1) does not propagate at all or (2) arrests at a length smaller than the radius of the NW. However, crack initiation has detrimental

effects on the system in that it can (1) increase the electrical resistance of the system and/or (2) increase the susceptibility of the NW to complete delamination upon subsequent external mechanical loading. We also find that the energy release rate is independent of the aspect ratio but increases linearly with the radius of the NW. Furthermore, we find that plasticity in the NW during lithiation significantly affects the energy release rate; materials with relatively low yield strengths limit the stresses build up in the system, thus reducing crack-driving forces. As a final note, our analysis of crack initiation depends on the value of the interfacial energy of the NW/CC interface. Because relatively few interfacial energies have been determined in these systems, we hope this study will motivate future experimental and first-principles simulations to determine the interfacial energies of materials of practical relevance in LIB systems.

ACKNOWLEDGEMENTS

The authors acknowledge the Texas A&M Engineering Experiment Station for funding. They also thank Geoffrey Garner for computing support.

REFERENCES

1. J.M. Tarascon and M. Armand, *Nature* 414, 359 (2001).
2. M. Armand and J.M. Tarascon, *Nature* 451, 652 (2008).
3. M.S. Whittingham, *MRS Bull.* 33, 411 (2008).
4. R. Marom, S.F. Amalraj, N. Leifer, D. Jacob, and D. Aurbach, *J. Mater. Chem.* 21, 9938 (2011).
5. W.-J. Zhang, *J. Power Sources* 196, 13 (2011).
6. M.N. Obrovac and L. Christensen, *Electrochem. Solid State Lett.* 7, A93 (2004).
7. U. Kasavajjula, C. Wang, and A.J. Appleby, *J. Power Sources* 163, 1003 (2007).
8. S.-B. Son, J.E. Trevey, H. Roh, S.-H. Kim, K.-B. Kim, J.S. Cho, J.-T. Moon, C.M. DeLuca, K.K. Maute, M.L. Dunn, H.N. Han, K.H. Oh, and S.-H. Lee, *Adv. Energy Mater.* 1, 1199 (2011).
9. S.D. Beattie, D. Larcher, M. Morcrette, B. Simon, and J.-M. Tarascon, *J. Electrochem. Soc.* 155, A158 (2008).
10. R. Deshpande, M. Verbrugge, Y.-T. Cheng, J. Wang, and P. Liu, *J. Electrochem. Soc.* 159, A1730 (2012).
11. S.P.V. Nadimpalli, V.A. Sethuraman, S. Dalavi, B. Lucht, M.J. Chon, V.B. Shenoy, and P.R. Guduru, *J. Power Sources* 215, 145 (2012).
12. C.S. Kang, S.-B. Son, J.W. Kim, S.C. Kim, Y.S. Choi, J.Y. Heo, S.-S. Suh, Y.-U. Kim, Y.Y. Chu, J.S. Cho, S.-H. Lee, and K.H. Oh, *J. Power Sources* 267, 739 (2014).
13. T. Takamura, S. Ohara, M. Uehara, J. Suzuki, and K. Sekine, *J. Power Sources* 129, 96 (2004).
14. C.K. Chan, H. Peng, G. Liu, K. McIlwrath, X.F. Zhang, R.A. Huggins, and Y. Cui, *Nat. Nanotechnol.* 3, 31 (2008).
15. H. Wu, G. Zheng, N. Liu, T.J. Carney, Y. Yang, and Y. Cui, *Nano Lett.* 12, 904 (2012).
16. R. Teki, M.K. Datta, R. Krishnan, T.C. Parker, T.-M. Lu, P.N. Kumta, and N. Koratkar, *Small* 5, 2236 (2009).
17. H.T. Nguyen, F. Yao, M.R. Zamfir, C. Biswas, K.P. So, Y.H. Lee, S.M. Kim, S.N. Cha, J.M. Kim, and D. Pribat, *Adv. Energy Mater.* 1, 1154 (2011).
18. B. Laïk, L. Eude, J.-P. Pereira-Ramos, C.S. Cojocaru, D. Pribat, and E. Rouvière, *Electrochim. Acta* 53, 5528 (2008).
19. K. Zhao, M. Pharr, J.J. Vlassak, and Z. Suo, *J. Appl. Phys.* 109, 016110 (2011).
20. A.R. Armstrong, G. Armstrong, J. Canales, R. García, and P.G. Bruce, *Adv. Mater.* 17, 862 (2005).
21. M.S. Park, G.X. Wang, Y.M. Kang, D. Wexler, S.X. Dou, and H.K. Liu, *Angew. Chem.* 119, 764 (2007).
22. Y. Li, B. Tan, and Y. Wu, *Nano Lett.* 8, 265 (2008).
23. J.Y. Huang, L. Zhong, C.M. Wang, J.P. Sullivan, W. Xu, L.Q. Zhang, S.X. Mao, N.S. Hudak, X.H. Liu, A. Subramanian, H. Fan, L. Qi, A. Kushima, and J. Li, *Science* 330, 1515 (2010).
24. T. Kennedy, E. Mullane, H. Geaney, M. Osiak, C. O'Dwyer, and K.M. Ryan, *Nano Lett.* 14, 716 (2014).
25. I. Ryu, J.W. Choi, Y. Cui, and W.D. Nix, *J. Mech. Phys. Solids* 59, 1717 (2011).
26. X.H. Liu, H. Zheng, L. Zhong, S. Huang, K. Karki, L.Q. Zhang, Y. Liu, A. Kushima, W.T. Liang, J.W. Wang, J.-H. Cho, E. Epstein, S.A. Dayeh, S.T. Picraux, T. Zhu, J. Li, J.P. Sullivan, J. Cumings, C. Wang, S.X. Mao, Z.Z. Ye, S. Zhang, and J.Y. Huang, *Nano Lett.* 11, 3312 (2011).
27. S. Huang and T. Zhu, *J. Power Sources* 196, 3664 (2011).
28. B. Jerliu, E. Hüger, L. Dörrer, B.K. Seidlhofer, R. Steitz, V. Oberst, U. Geckle, M. Bruns, and H. Schmidt, *J. Phys. Chem. C* 118, 9395 (2014).
29. M. Pharr, K. Zhao, X. Wang, Z. Suo, and J.J. Vlassak, *Nano Lett.* 12, 5039 (2012).
30. M.T. McDowell, S.W. Lee, J.T. Harris, B.A. Korgel, C. Wang, W.D. Nix, and Y. Cui, *Nano Lett.* 13, 758 (2013).
31. J.W. Wang, Y. He, F. Fan, X.H. Liu, S. Xia, Y. Liu, C.T. Harris, H. Li, J.Y. Huang, S.X. Mao, and T. Zhu, *Nano Lett.* 13, 709 (2013).
32. L. Chen, F. Fan, L. Hong, J. Chen, Y. Ji, S. Zhang, T. Zhu, and L. Chen, *J. Electrochem. Soc.* 161, F3164 (2014).
33. Y.S. Choi, M. Pharr, K.H. Oh, and J.J. Vlassak, *J. Power Sources* 294, 159 (2015).
34. K. Zhao, M. Pharr, J.J. Vlassak, and Z. Suo, *J. Appl. Phys.* 108, 073517 (2010).
35. Y.S. Choi, M. Pharr, K.H. Oh, and J.J. Vlassak, *J. Power Sources* 294, 159 (2015).
36. M.E. Stournara, X. Xiao, Y. Qi, P. Johari, P. Lu, B.W. Sheldon, H. Gao, and V.B. Shenoy, *Nano Lett.* 13, 4759 (2013).